Generation of broadband two-dimensional multicolored arrays in a sapphire plate

Jun Liu [1, 2], Takayoshi Kobayashi [1, 2, 3, 4, *], and Zhiguang Wang[1]

1Department of Applied Physics and Chemistry and Institute for Laser Science, University of Electro-Communications, Chofugaoka 1-5-1, Chofu, Tokyo 182-8585 Japan
2 International Cooperative Research Project (ICORP), Japan Science and Technology Agency, 4-1-8 Honcho, Kawaguchi, Saitama 332-0012, Japan
3Department of Electrophysics, National Chiao Tung University, 1001 Ta Hsueh Rd. Hsinchu 300, Taiwan
4 Institute of Laser Engineering, Osaka University, Yamadakami 2-6, Suita 565-0871, Ibaraki 567-0047, Japan
**Corresponding author: kobayashi@ils.uec.ac.jp,*

Abstract: Broadband 2-D multicolored arrays with more than ten periodic columns and more than ten rows were generated in a sapphire plate using two crossed femtosecond laser beams overlapping in time and space. These multicolored 2-D arrays were sensitive to rotation of the sapphire plate in the plane normal to the incident beams. The broadband spectrum, pulse duration less than 40fs, and less than 1%RMS power stability of the array signals make them well suited for various applications, for example multicolor pump-probe experiments.

OCIS codes: (190.4380) Nonlinear optics, four-wave-mixing; (320, 2250) Femtosecond phenomena; (190, 7110) Ultrafast nonlinear optics; (190.4420) Nonlinear optics, transverse effects in.

References and links

1. A. Saliminia, S. Chin, and R. Vallée, "Ultra-broad and coherent white light generation in silica glass by focused femtosecond pulses at 1.5 um," Opt. Express **13**, 5731-5738 (2005).
2. M. Segev and G. Stegeman, "Self-Trapping of Optical Beams: Spatial Solitons," Phys. Today **51**, 43-48 (1998).
3. C. G. Durfee III, S. Backus, M. M. Murnane, and H. C. Kapteyn, "Ultrabroadband phase-matched optical parametric generation in the ultraviolet by use of guided waves," Opt. Lett. **22**, 1565-1567 (1997).
4. C. Conti, S. Trillo, P. Di Trapani, G. Valiulis, A. Piskarskas, O. Jedrkiewicz, and J. Trull, "Nolinear electromagnetic X waves," Phys. Rev. Lett. **90**, 170406 (2003).
5. T. Kobayashi, A. Shirakawa, and T. Fuji, "Sub-5-fs transform-limited visible pulse source and its application to real-time spectroscopy," IEEE J. Sel. Top. Quantum Electron. **7**, 525-538 (2001).
6. H. Crespo, J. T. Mendonça, and A. Dos Santos, "Cascaded highly nondegenerate four-wave-mixing phenomenon in transparent isotropic condensed media," Opt. Lett. **25**, 829-831 (2000).
7. J. Liu and T. Kobayashi, "Wavelength-tunable multicolored femtosecond laser pulse generation in fused silica glass," Opt. Lett. **34**, 1066-1068 (2009).
8. J. Liu and T. Kobayashi, "Generation of uJ-level multicolored femtosecond laser pulses using cascaded four-wave mixing," Opt. Express **17**, 4984-4990 (2009).
9. J. Liu and T. Kobayashi, "Cascaded four-wave mixing and multicolored arrays generation in a sapphire plate by using two crossing beams of femtosecond laser," Opt. Express **16**, 22119-22125 (2008).
10. M. Zhi and A. V. Sokolov, "Broadband coherent light generation in a Raman-active crystal driven by two-color femtosecond laser pulses," Opt. Lett. **32**, 2251-2253 (2007).
11. E. Matsubara, T. Sekikawa, and M. Yamashita, "Generation of ultrashort optical pulses using multiple coherent anti-Stokes Raman scattering in a crystal at room temperature," Appl. Phys. Lett. **92**, 071104 (2008).
12. H. Matsuki, K. Inoue, and E. Hanamura, "Multiple coherent anti-Stokes Raman scattering due to phonon grating in KNbO3 induced by crossed beams of two-color femtosecond pulses," Phys. Rev. B **75**, 024102 (2007)
13. K. Inoue, J. Kato, E. Hanamura, H. Matsuki, and E. Matsubara, "Broadband coherent radiation based on peculiar multiple Raman scattering by laser-induced phonon grating in TiO2," Phys. Rev. B **76**, 041101(R) (2007).
14. E. Matsubara, K. Inoue, and E. Hanamura, "Violation of Raman selection rules induced by two femtosecond laser pulses in KTaO3," Phys. Rev. B **72**, 134101 (2005).

#108884 - $15.00 USD Received 17 Mar 2009; revised 21 Apr 2009; accepted 22 Apr 2009; published 18 May 2009

15. J. Liu, J. Zhang, and T. Kobayashi, "Broadband coherent anti-Stokes Raman scattering light generation in BBO crystal by using two crossing femtosecond laser pulses," Opt. Lett. **33**, 1494-1496 (2008).
16. D. Faccio, A. Dubieties, G. Tamosauskas, P. Polesana, G. Valiulis, A. Piskarskas, A. Lotti, A. Couairon, and P. Di Trapani, "Phase- and group-matched nonlinear interactions mediated by multiple filamentation in Kerr media," Phys. Rev. A **76**, 055802 (2007).
17. D. Kip, M. Soljacic, M. Segev, E. Eugenieva, and D. N. Christodoulides, "Modulation instability and pattern formation in spatially incoherent light beams," Science **290**, 495-498 (2000).
18. J.W. Fleischer, M. Segev, N. K. Efremidis, and D. N. Christodoulides, "Observation of two-dimensional discrete solutions in optically induced nonlinear photonic lattices," Nature **422**, 147-150 (2003).
19. X. Wang, A. Bezryadina, Z. Chen，K. G. Makris, D. N. Christodoulides, and G. I. Stegeman，"Observation of Two-Dimensional Surface Solitons," Phys. Rev. Lett. **98**, 123903 (2007).
20. H. Zeng, J. Wu, H. Xu, and K. Wu, "Generation and weak beam control of two-dimensional multicolored arrays in a quadratic nonlinear medium," Phys. Rev. Lett. **96**, 083902 (2006).
21. V. Kartazaev, and R. R. Alfano, " Polarization properties of SC generated in CaF2," Opt. Commun. **281**, 463-468 (2008).
22. P. B. Lundquist, D. R. Andersen, and Y. S. Kivshar, "Multicolor solitons due to four-wave mixing," Phys. Rev. E **57**, 3551–3555 (1998).
23. G. Fanjoux, J. Michaud, M. Delqu´e, H. Mailotte, and T. Sylvestre, "Generation of multicolor vector Kerr solitons by cross-phase modulation, four-wave mixing, and stimulated Raman scattering," Opt. Lett. **31**, 3480–3482 (2006).

1. Introduction

When an ultrashort pulse propagates in a nonlinear bulk medium, various nonlinear optical phenomena such as supercontinuum light generation [1], optical solitons [2], optical parametric generation [3], and X-wave generation [4] have been observed. When two ultrashort pulses that overlap in space and time propagate in a nonlinear bulk medium, much more interesting nonlinear optical phenomena have appeared. Optical parametric amplification based on a nonlinear crystal is well established, and has been used for many scientific experiments [5]. A 1-D broadband multicolored sideband array was observed when two crossed femtosecond beams were synchronized in BK7 glass [6], fused silica glass [7-8], sapphire [9] and certain crystals, for example $PbWO_4$ [10], $LiNbO_3$ [11], $KNbO_3$ [12], TiO_2 [13], $KTaO_3$ [14], and BBO [15]. However, all these phenomena occurred in one dimension only. There were only few experiments based on 2-D nonlinear optical phenomena. 2-D arrays of transverse patterns were experimentally observed in the multifilament interactions [16, 17], and 2-D solitons were the subject of considerable research over the last decade. Two-dimensional discrete solitons [18] and surface solitons [19] were observed in nonlinear photonic lattices. Regular 2-D multicolored transverse arrays were also observed when two crossed femtosecond laser beams were synchronized in a quadratic nonlinear crystal [20]. We recently reported the observation of 2-D multicolored arrays in a sapphire plate [9], while only 5 rows of arrays were generated and only the spectrum property is studied in that paper. The data are not enough to understand this new phenomenon and to make use of the 2-D multicolored sidebands.

In this letter, we reported the generation of stable broadband 2-D multicolored arrays with more than ten periodic columns and more than ten rows in a sapphire plate using two crossed femtosecond laser beams overlapping in time and space. The properties of the spectrum, spatial mode, power stability, polarization, pulse duration and crossing angle between two neighbor sidebands of the 2-D muliticolored arrays were studied in detail. These researches will help people to understand the process and explain the phenomenon in the future. These data also clarify the possibility of the many kinds of applications of the generated sidebands. Moreover, we found that these stable 2-D multicolored arrays were sensitive to the orientation of the optical axis of the sapphire plate with respect to the plane of polarization of the incident beams. This is an interesting phenomenon that makes it possible to control the 2-D multicolor arrays using polarizer optics or rotating the sapphire plate.

#108884 - $15.00 USD Received 17 Mar 2009; revised 21 Apr 2009; accepted 22 Apr 2009; published 18 May 2009

2. Experiment setup

A 1kHz Ti:sapphire regenerative amplifier fs laser system (Micra+Legend-USP, Coherent) with 40 fs pulse duration and 2.5 W average output power was used as a pump source. The laser pulse after the regenerative amplifier system was split into three beams using beam splitters. One of the beams (beam_1) was spectrally broadened in a hollow fiber with a 250 μm inner-diameter and 60 cm in length that was filled with krypton gas. The broadband spectrum after the hollow fiber was dispersion compensated with a pair of chirped mirrors and a pair of glass wedges. The pulse duration after the hollow fiber compressor was about 10 fs. After passing through a bandpass filter at 720 nm, beam_1 was focused into a 2-mm-thick sapphire plate by a concave mirror with 60cm focal length. Another beam (beam_2) passed through a delay stage with less than 3 fs resolution. Beam_2 was first attenuated by a variable neutral density (VND) filter and was then focused into the sapphire plate by a lens with 1m focal length. The third beam (beam_3) was used to generate correlation signals with the input beams and the generated sidebands in a 10-μm-thick BBO crystal, which was used to measure pulse durations.

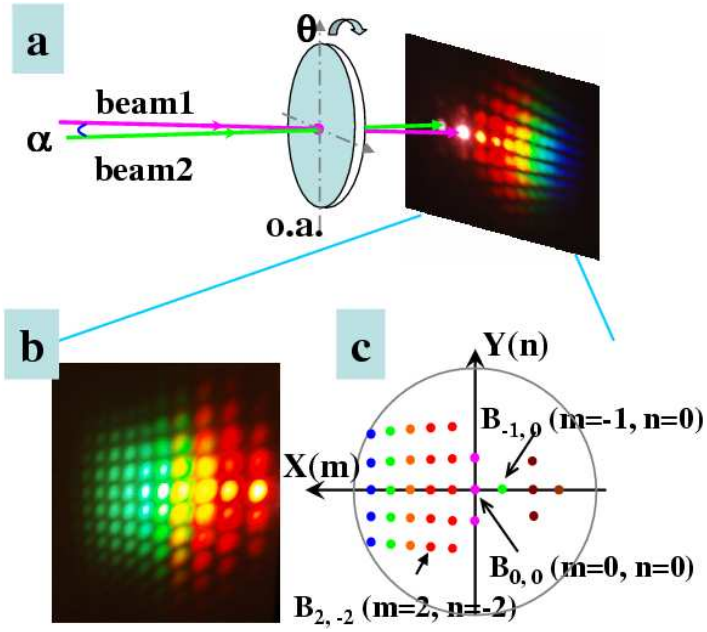

Fig. 1. (a) Schematics of the experimental setup for multicolored array generation. α is the crossing angle between the two input beams, beam_1 and beam_2 in the air. θ is the rotation angle of the sapphire plate. (b) A photograph of the 2-D multicolored array on a UV light sensitive plate. (c) Definition of 2-D multicolored arrays, where $B_{0,0}$ and $B_{-1,0}$ refer to two incident beams, beam_1 and beam_2, respectively.

Schematics of the experimental setup for multicolored array generation are shown in Fig. 1(a). The sapphire plate was a-cut and there were two orthogonal optical axes in the plane of the sapphire plate. The plane formed by the two orthogonal crystal axes was set normal to the two input beams. The two input beams had perpendicular polarizations and coincided with one of the crystal axes. The diameters of both incident beams on the surface of sapphire plate were 300 μm, as initially measured by a CCD camera (BeamStar FX 33, Ophir Optronics). The crossing angle α between the two input beams was $1.8^{o} \pm 0.02^{o}$ in the air. When beam_1 and beam_2 were synchronously focused on the sapphire plate in both time and space, stable separate 2-D transverse multicolored array signals at different wavelengths were generated. The polarizations of the multicolored arrays were the same as those of the input beams as

#108884 - $15.00 USD Received 17 Mar 2009; revised 21 Apr 2009; accepted 22 Apr 2009; published 18 May 2009

tested using a film polarizer. Figure 1(b) shows a photograph of the 2-D multicolored arrays on a UV light sensitive plate placed about 20 cm after the sapphire plate. More than ten quasi-periodic columns and more than ten rows of multicolor signals can be seen, well separated from each other in space. The columns approximately normal to the center row and the rows adjacent to the center row were not parallel to the center row. For convenience, the 2-D multicolored array signals were defined to be $B_{m, n}$, as shown in Fig. 1(c), where $B_{0, 0}$ and $B_{-1, 0}$ refer to two incident beams, beam_1 and beam_2, respectively. There were also two sidebands, $B_{-2, 1}$ and $B_{-2, -1}$, beside the first-order Stokes sideband $B_{-2, 0}$. The divergence angle of the sidebands was measured using a paper 50 cm after the sapphire plate to mark the position of each sideband. Neighboring spots on the same column have nearly the same crossing angle. However, the angle between two neighboring signals was decreased from 2.2° to 0.7° in the x direction (row direction, Fig. 1(c)) and from 1.7° to 1.0° in the y direction (column direction, Fig. 1(c)) as the sidebands changed from column $B_{-2, n}$ to the $B_{7, n}$ column.

3. Experimental results and discussion

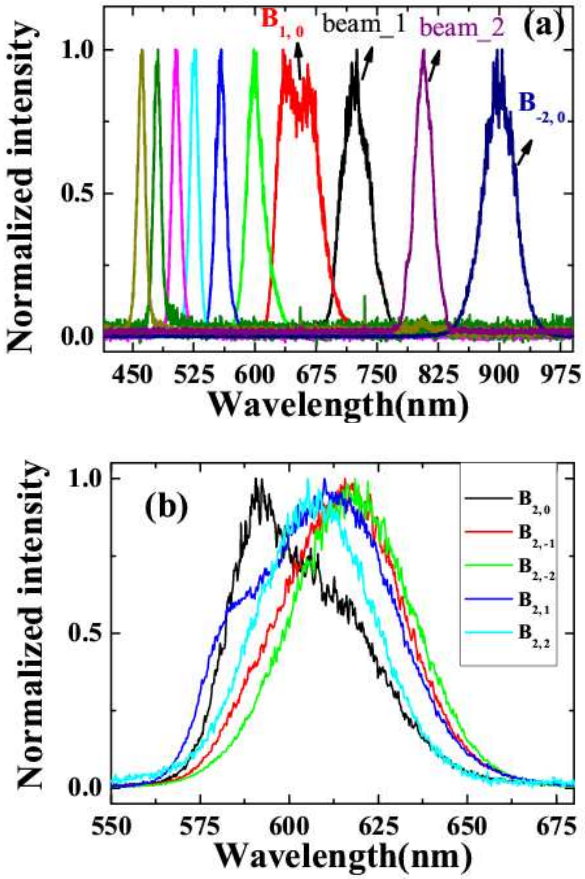

Fig. 2. (a) The spectra of array signals on the center row $B_{m, 0}$, where beam_1 and beam_2 are two incident beams. (b) The spectra of array signals on the second column $B_{2, n}$.

The spectra of array signals on the center row $B_{m, 0}$ were measured using a multichannel spectrometer (USB4000, Ocean Optics), as shown in Fig. 2(a). For clarity, not all sideband spectra are shown. A broadband spectrum from 400 nm to 1.2 μm with more than 1.5 octaves was generated [9]. These generated sidebands were explained to be the result of a cascaded

#108884 - $15.00 USD Received 17 Mar 2009; revised 21 Apr 2009; accepted 22 Apr 2009; published 18 May 2009

FWM process, which was recently reported in detail [6-9]. The spectra were tunable by changing the crossing angle α between the two input beams, and also by changing the center wavelength of the bandpass filter. The maximum difference between peak wavelengths of the side spots and the center spot on the same column was about 20 nm, as shown in Fig. 2 (b).

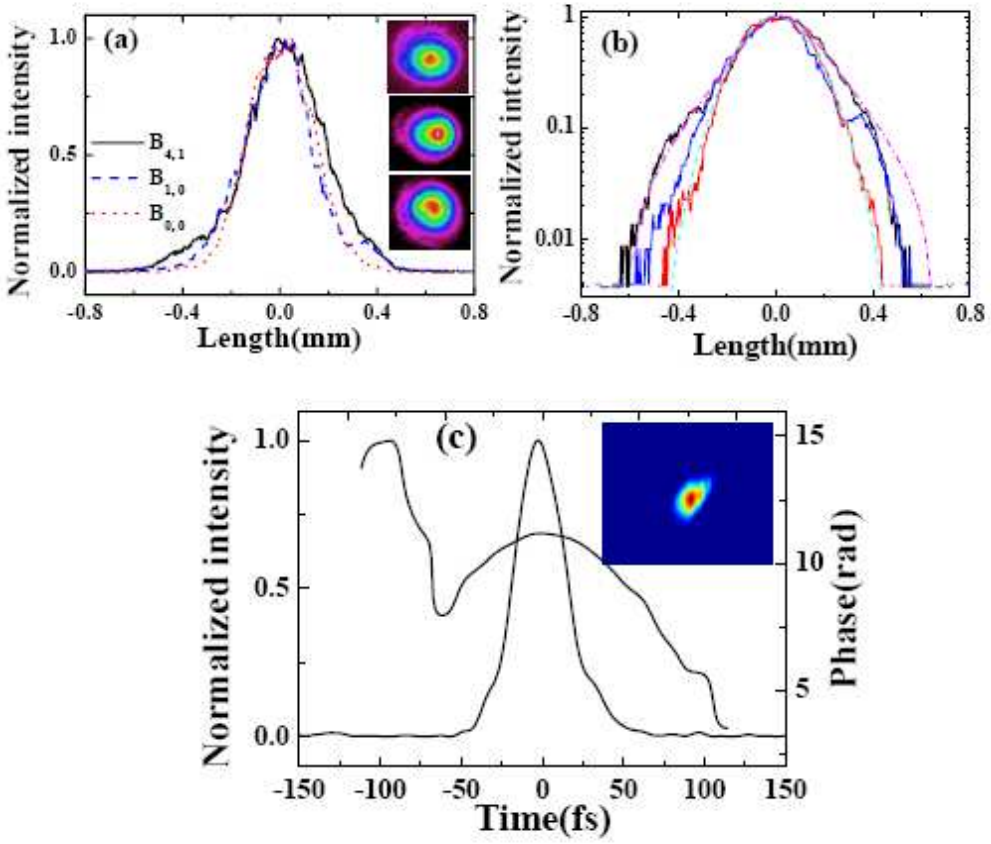

Fig. 3. (a) The spatial profiles of $B_{0,0}$, $B_{1,0}$, and $B_{4,1}$ in one dimension. The inset patterns are spatial modals of $B_{0,0}$, $B_{1,0}$, and $B_{4,1}$ from bottom to top, measured by a CCD camera. (b) The spatial profiles of $B_{0,0}$, $B_{1,0}$, and $B_{4,1}$ in one dimension with logarithmic scale in the intensity. The cyan dashed line is the Gaussian fit of $B_{0,0}$. The magenta dash-dotted line is the Lorentzian fit of $B_{4,1}$. (c) The retrieved XFROG pulse trace and phase of the $B_{1,0}$ with a retrieved error of 0.01022. The retrieved pulse duration is 35 ± 3fs. The inset pattern is the measured XFROG trace.

The spatial profiles of different signals in the arrays were measured using a CCD camera. Figure 3(a) shows spatial profiles of $B_{0,0}$, $B_{1,0}$, and $B_{4,1}$ in two dimensions and one dimension. Figure 3(b) shows one-dimensional spatial profiles of $B_{0,0}$, $B_{1,0}$, and $B_{4,1}$ with logarithmic scale in the intensity. The spatial profile changed from Gaussian ($B_{0,0}$) to a Lorentzian profiles ($B_{4,1}$). The cyan dashed line in Fig. 3(b) is the Gaussian fit of $B_{0,0}$. The magenta dash-dotted line in Fig. 3(b) is the Lorentzian fit of $B_{4,1}$. The pulse duration of the sidebands were measured by cross-correlation with beam_3. Figure 3(c) shows the retrieved XFROG pulse trace and the phase of $B_{1,0}$ with a retrieved error of 0.01022 from the commercial software from Femtosoft Technologies. The retrieved pulse duration was 35 ± 3 fs. The retrieved phase shows that there was some chirp in the pulse due to the positive chirped input pulses and the dispersion of the glass. The pulse duration of $B_{1,0}$ was even shorter than the two incident pulses, the cross-correlation width of which with beam_3 were

#108884 - $15.00 USD Received 17 Mar 2009; revised 21 Apr 2009; accepted 22 Apr 2009; published 18 May 2009

82 ± 5 fs and 84 ± 5 fs for beam_1 and beam_2 due to the dispersion of the filter and lens, respectively.

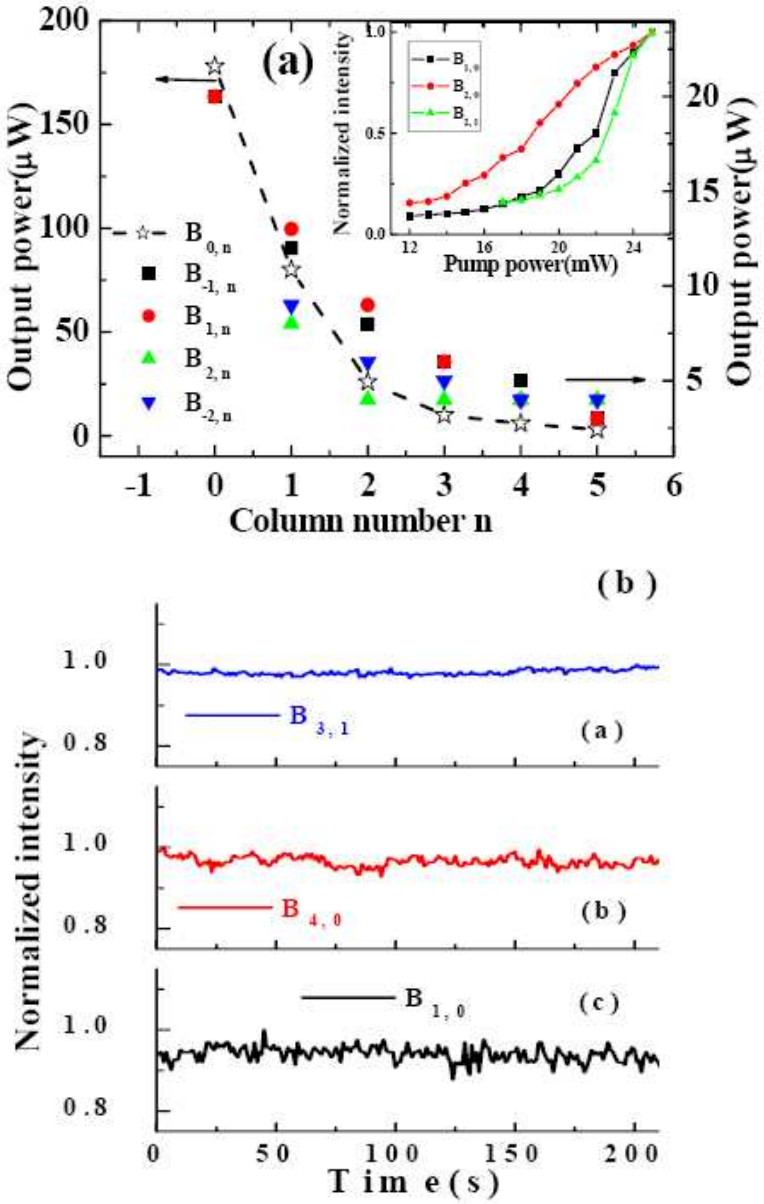

Fig. 4. (a) The output power of array signals on the 0, ±1, and ±2 rows when the power of the two incident beams, beam_1 and beam_2, were 0.1mW and 25mW, respectively. Only the signals in the center row are marked with star symbols and dashed line, as shown on the left. The inset figure shows the dependence of the output power of different sidebands on the input power of beam_2. (b) The power stabilities of $B_{4,0}$, $B_{3,1}$, and $B_{1,0}$ monitored for 200 seconds, which were 1.25%RMS, 0.63%RMS, and 1.84% RMS, respectively.

We measured the powers of some array signals when the power of the two incident beams, beam_1 and beam_2, were 0.1 mW and 25 mW, respectively, as shown in Fig. 4(a). The signal power decreased rapidly with increasing column order for signals on the center row $B_{m,0}$, as shown by the star symbols in Fig. 4(a). The difference in output power between the side

#108884 - $15.00 USD Received 17 Mar 2009; revised 21 Apr 2009; accepted 22 Apr 2009; published 18 May 2009

spots and the center spot on the same column decreased continuously as the row order increased. For signals on column 5 ($B_{5,n}$), signal power on the center row $B_{5,0}$ was even smaller than that on rows ±1 and ±2. The dependence of the different sideband output power on the input power of beam_2 is shown in the inset of Fig. 4(a). The increase in signal power with higher column or row order was delayed, but more rapid than that of lower order columns or rows. In this case, the power of beam_1 was very low, and saturation did not take place. In fact, the output power of beam_1 was amplified from 0.1 mW to 0.17 mW in the experiment. The power stabilities of different array signals were monitored by a Si power sensor, as shown in Fig. 4(b). The stability of $B_{1,0}$ was about 1.84% RMS over 200 seconds. Interestingly, the stabilities of the high order sidebands were much better than that of the first-order, especially for the sidebands beside the beam on the center row. The stabilities of $B_{4,0}$, $B_{3,1}$, and $B_{4,1}$ were 1.25%RMS, 0.63% RMS, and 0.97% RMS over 200 seconds, respectively.

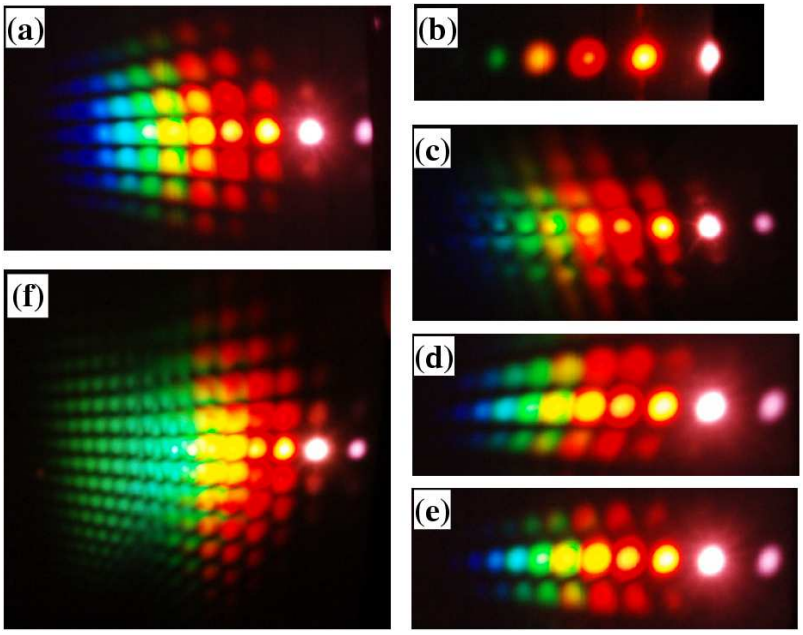

Fig. 5. Photographs of 2-D multicolored arrays on a sheet of white paper when (a) the plane of polarization of the two input beams coincided with one of the crystal axes; (b) the sapphire plate rotated for 45°; (c) noise pattern; (d) and (e) show photographs with the sapphire plate rotated by -16° and 14°, respectively. (f) A photograph of the 2-D multicolored arrays on a UV light sensitive plate when the input power of beam_2 was increased to 27mW.

We observed the multicolored arrays to be sensitive to the rotation of the sapphire plate in the plane normal to the input beams. The brightest and largest number of array signals appeared when the plane of the polarization of the two input beams coincided with one of the crystal axes, as shown in Fig. 5(a). It need to clarify that the white color of the two input beams due to the over exposure of camera. There is no white light generation in the two input beams. It was found that there were four angles 0°, 90°, 180°, and 270° at which the sidebands were brightest, and four angles 45°, 135°, 225°, and 315° at which the sidebands were weakest, as shown in Fig. 5(b). The periodic array did not appear continuously but appeared aperiodically *i.e.* when the angle was rotated 6°, 14°, 0°, -6°, -11°, -13°, -16°, and -19° and further. At other angles, these regular arrays were replaced by a noise pattern, as shown in Fig. 5(c). The rotation angle of the sapphire plate also affected the position of the array signals. Figures 5(d) and 5(e) showed photographs when the sapphire plate was rotated by -16° and 14°, respectively. It can be seen that the column line was tilted a different direction when the sapphire plate was rotated. The spectrum of the tilted signal was slightly narrower in

#108884 - $15.00 USD Received 17 Mar 2009; revised 21 Apr 2009; accepted 22 Apr 2009; published 18 May 2009

the shorter wavelength region when the signal was tilted in the high order direction, and vice versa. If the power of beam_2 was increased to 27 mW, bright stable "fish-like" multicolor arrays were observed, as shown in Fig. 5(f).

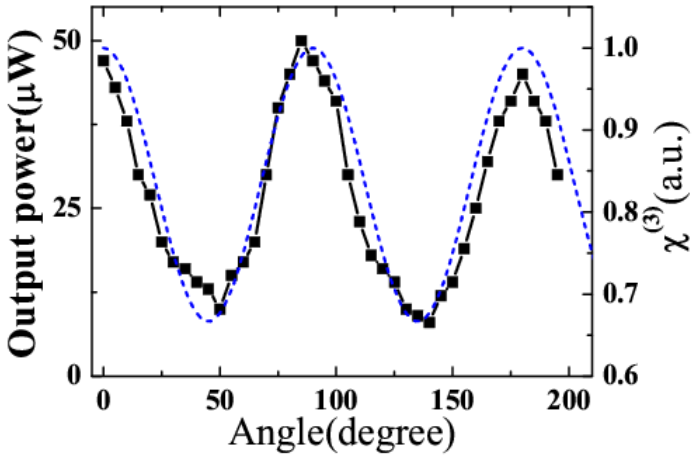

Fig. 6. The dependence of $B_{1,0}$ output power (square symbols) and $|\chi^{(3)}(\theta)|$ (dashed line)of the sapphire plate on the rotation angle θ of the sapphire plate.

The dependence of the $B_{1,0}$ output power on the rotation angle θ of the sapphire plate was measured, as shown in Fig. 6. Here we only show the evolution in the rotation angle region from 0^o to 210^o. Clearly, the output power changed periodically with rotation of the sapphire plate. This periodic evolution was because of the periodic dependence of $\chi^{(3)}(\theta) \propto \cos^2(2\theta)$ +1of the sapphire plate on the rotation angle θ, as shown by the dashed line in Fig. 6. The peak wavelength of the sidebands shifted continuously to a shorter wavelength by about 20 nm when the sapphire plate was rotated from 0^o to 45^o due to a phase matching condition. The polarization of the sidebands also changed with rotation of the sapphire plate. To detect the polarization rotation of the sidebands, a thin film polarizer was located normal to the sideband beams and placed 50 cm after the sapphire plate. The polarizations of the multicolored arrays were the same as those of the input beams when the plane of polarization of the input beams coincided with one of the crystal axes. Very little orthogonally polarized light was detected. As the sapphire plate was rotated from 0^o to 90^o, the orthogonally polarized light continuously increased from 0^o to 45^o and decreased from 45^o to 90^o, and light with parallel polarization showed the opposite effect. At 45^o, the sidebands were the weakest, and the orthogonally polarized light had power equal to the parallel polarized light. We rotated the thin film polarizer to minimize the intensity of light passing through the film polarizer. The rotation angle of the thin film polarizer β was in accordance with the rotation angle of the sapphire plate θ, and had the same angle when the sapphire plate was rotated from 0^o to 45^o and was 90^o - θ when the sapphire plate was rotated from 45^o to 90^o. This rotation angle dependence phenomenon was also recently observed in supercontinuum generation process [21]. The physical explanation of the phenomenon is complex because it included combined effects of the cascaded third-order nonlinear processes of FWM, coherent anti-Stokes Raman scattering (CARS), cross-phase modulation (XPM), and self-phase modulation (SPM) [22-23]. Much detail physical explanation of this phenomenon will be explored in the future.

A half-wave plate or a quartz-wave plate can also be used in the path of one of the input beams to safely control the multicolored arrays. The polarization, intensity, and position of the multicolored arrays can be controlled by rotating the sapphire plate. Note that this phenomenon did not appear when a fused silica glass was used as the medium, due to its

#108884 - $15.00 USD Received 17 Mar 2009; revised 21 Apr 2009; accepted 22 Apr 2009; published 18 May 2009

symmetric structure. This phenomenon was very easily repeated in the experiment, and the sapphire plate was not damaged over the course of the experiment.

4. Conclusion

In conclusion, an interesting 2-D nonlinear optical phenomenon was observed. Broadband femtosecond 2-D multicolored arrays with more than ten periodic columns and more than ten rows were generated in a sapphire plate. These stable 2-D multicolored arrays can be controlled by rotating the sapphire plate, a half-wave plate, or a quarter wave plate. The properties of the spectrum, spatial modal, power stability, and pulse duration of the 2-D multicolored arrays show they could be used in various applications, for example 2-D all-optical switching devices or multicolor pump-probe experiments.

Acknowledgment

The authors thank Prof. G. I. Stegeman for his valuable discussion. This work was partly supported by the 21st Century COE program on “Coherent Optical Science” and partly supported by the grant from the Ministry of Education (MOE) in Taiwan under the ATU Program at National Chiao Tung University. A part of this work was performed under the joint research project of the Laser Engineering, Osaka University, under contract subject B1-27.

#108884 - $15.00 USD Received 17 Mar 2009; revised 21 Apr 2009; accepted 22 Apr 2009; published 18 May 2009